Structural anomaly and dynamic heterogeneity in cycloether/water binary mixtures: Signatures from composition dependent dynamic fluorescence measurements and computer simulations

Sandipa Indra, Biswajit Guchhait, and Ranjit Biswas

Citation: J. Chem. Phys. **144**, 124506 (2016); doi: 10.1063/1.4943967
View online: http://dx.doi.org/10.1063/1.4943967
View Table of Contents: http://aip.scitation.org/toc/jcp/144/12
Published by the American Institute of Physics

Structural anomaly and dynamic heterogeneity in cycloether/water binary mixtures: Signatures from composition dependent dynamic fluorescence measurements and computer simulations

Sandipa Indra, Biswajit Guchhait, and Ranjit Biswas[a)]
Department of Chemical, Biological and Macromolecular Sciences, S. N. Bose National Centre for Basic Sciences, Block-JD, Sector-III, Salt Lake, Kolkata 700098, India

(Received 14 December 2015; accepted 1 March 2016; published online 24 March 2016)

We have performed steady state UV-visible absorption and time-resolved fluorescence measurements and computer simulations to explore the cosolvent mole fraction induced changes in structural and dynamical properties of water/dioxane (Diox) and water/tetrahydrofuran (THF) binary mixtures. Diox is a quadrupolar solvent whereas THF is a dipolar one although both are cyclic molecules and represent cycloethers. The focus here is on whether these cycloethers can induce stiffening and transition of water H-bond network structure and, if they do, whether such structural modification differentiates the chemical nature (dipolar or quadrupolar) of the cosolvent molecules. Composition dependent measured fluorescence lifetimes and rotation times of a dissolved dipolar solute (Coumarin 153, C153) suggest cycloether mole-fraction ($X_{THF/Diox}$) induced structural transition for both of these aqueous binary mixtures in the $0.1 \leq X_{THF/Diox} \leq 0.2$ regime with no specific dependence on the chemical nature. Interestingly, absorption measurements reveal stiffening of water H-bond structure in the presence of both the cycloethers at a nearly equal mole-fraction, $X_{THF/Diox} \sim 0.05$. Measurements near the critical solution temperature or concentration indicate no role for the solution criticality on the anomalous structural changes. Evidences for cycloether aggregation at very dilute concentrations have been found. Simulated radial distribution functions reflect abrupt changes in respective peak heights at those mixture compositions around which fluorescence measurements revealed structural transition. Simulated water coordination numbers (for a dissolved C153) and number of H-bonds also exhibit minima around these cosolvent concentrations. In addition, several dynamic heterogeneity parameters have been simulated for both the mixtures to explore the effects of structural transition and chemical nature of cosolvent on heterogeneous dynamics of these systems. Simulated four-point dynamic susceptibility suggests formation of clusters inducing local heterogeneity in the solution structure. © *2016 AIP Publishing LLC.* [http://dx.doi.org/10.1063/1.4943967]

I. INTRODUCTION

Due to nearly zero dipole moment ($\mu = 0.45\ D$),[1] continuum dielectric theory fails to predict the nuclear reorganization energy of nondipolar solvent 1,4-dioxane (Diox) in response to an altered charge distribution of a dissolved dipolar solute. Diox produces comparable fluorescence Stokes shift for solvatochromic probe Coumarin 153 (C153) to that in tetrahydrofuran (THF), a moderately dipolar solvent possessing a dipole moment of 1.75 D.[1] This unexpected observed shift for C153 in Diox was correlated[1] with the solute–solvent dipole–quadrupole and higher order multipole interactions. The chemical structures of these two solvents, THF and Diox (shown in Scheme 1), are similar and contain polar CH_2–O–CH_2 group/groups. But the molecular symmetry results in a negligible μ value for Diox. Another striking feature associated with these molecules is that aqueous solution of THF exhibits a closed immiscibility loop with a lower consolute temperature (LCST) of $T_L^C = 344$ K (superheated regime, boiling point of THF = 339 K) with critical concentration $X_{THF}^C = 0.225$ and an upper consolute temperature (UCST) of about $T_U^C = 410$ K,[2] whereas Diox is completely miscible in water at all temperatures[3] (boiling point of Diox = 374 K[4]). Despite the non-existence of a critical point for Diox/water system, aqueous solutions of both THF and Diox showed anomalous behaviour in thermodynamic properties,[5–9] ultrasonic velocity,[10] and absorption[11] and explained it in terms of concentration fluctuations.[5–11]

Correlation lengths associated with concentration fluctuations in these aqueous binary mixtures revealed by various experimental techniques differ significantly from one another. For example, laser light scattering[12] showed the existence of dynamic correlation length of ~200–600 nm, whereas small angle neutron scattering (SANS)[13,14] suggested the largest length of ~2 nm. Several other measurements such as Rayleigh light scattering,[15] low frequency Raman scattering,[16,17] nuclear magnetic resonance (NMR),[18,19] X-ray diffraction,[18] mass spectroscopy,[18,20] X-ray scattering,[13,21] dielectric relaxation[22–24] further reported on this aspect and observed different mixing schemes depending on concentration of these cycloethers in water. Raman scattering[16,17] studies showed that the tetrahedral H-bonding network of water collapses at $X_{ether} \sim 0.2$–0.3. While the

a)Author to whom correspondence should be addressed. Electronic mail: ranjit@bose.res.in. Tel.: 91 33 2335 5706. Fax: 91 33 2335 3477.

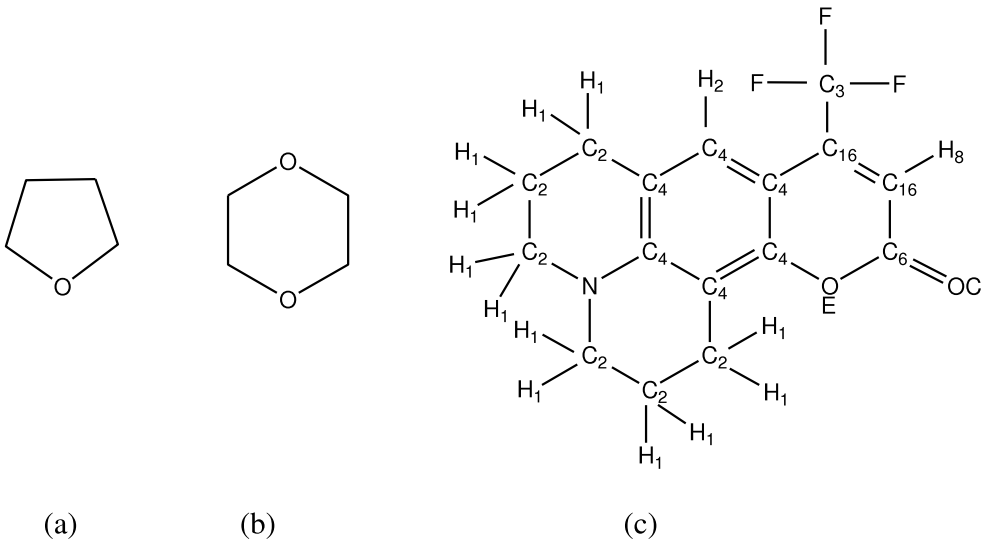

SCHEME 1. Chemical structures of (a) Tetrahydrofuran (THF), (b) 1,4-dioxane (Diox), and (c) Coumarin 153 (C153). Representation of different atomic sites of C153 is shown here as used in the simulations of radial distribution function (RDF).

effects of hydrophobic moieties on retaining the characteristic water structure were explored by mass spectroscopy,[20] NMR[19] measurements suggested hydrophobic moiety does not play any role in inducing anomalous polarization of water molecules; H-bonding basicity of the polar group is the determining factor here. Later, solvation dynamics study of different solvatochromic probes in Diox/water binary mixtures correlated the slower rotational diffusion of the Diox–water oligomeric species as the origin of the longer time scale.[25,26] In addition, solvent translation and preferential solvation have been predicted to affect the solvation rate in binary mixtures at long times.[27–30] Interestingly, dynamic light scattering (DLS)[31] study in THF/water mixtures reported growth of concentration fluctuation correlation length while approaching liquid–liquid lower critical solution point with a critical point exponent[32] value of 0.65 and the effect was prominent at room temperature which is far from the LCST. Similar kind of growth of the correlation length was also found in 2-butoxyethanol (BE)/water binary mixtures with a closed-loop miscibility gap,[33] but we observed no role for the critical fluctuations preceding phase separation from time-resolved fluorescence spectroscopic measurements.[34] Recent computer simulation study of THF/water mixture has suggested that subtle structural changes with temperature lead to the miscibility gap in this binary mixture.[35]

In aqueous solution, THF and Diox molecules do not participate in hydrogen bonding (H-bonding) interaction among themselves due to lack of donor hydrogen atoms, but they can form H-bonds with water by the acceptor oxygen atoms. Therefore, the study of aqueous solutions of these cycloethers provides an avenue to investigate how they affect the tetrahedral H-bond network structure of water. In steady-state absorption and fluorescence spectroscopic measurements, the added solute (usually present at $\leq 10^{-5}$M) reports on modification in the solute–medium interaction upon variation of concentration of the cosolvent in the binary mixture via changes in the spectral frequencies and widths. These spectral changes are a reflection of the cosolvent-induced changes in the equilibrium structure of the binary mixture. Time-resolved fluorescence measurements, on the other hand, inform on alteration of relaxation dynamics due to the structural changes in the solution. We would, however, like to mention here that although the composition dependent absorption and fluorescence spectroscopic changes are often interpreted in terms of solute-solvent direct interaction (a sort of nearest-neighbour events), these collective measurements sense modifications over large lengthscale where participation of many molecules takes place. In such a situation, computer simulations provide an effective tool for a detailed understanding of the interactions at the microscopic level. However, the presence of only few such studies[36–41] with the primary focus of most of them[39–41] being on the molecular mechanism of phase separation has not served the purpose. This has been the principal motivation for us to perform molecular dynamics (MD) simulation study along with spectroscopic (steady state and time-resolved) measurements of THF/water and Diox/water binary mixtures employing C153 as a solute probe (Scheme 1). In this study, the following solution aspects have been addressed: (i) whether the presence of critical point affects the structure of the solution differently, (ii) how the structural changes of the solution alters the dynamics (as reported by the probe solute) of these media, (iii) whether the modifications in solution structural and dynamical aspects bear any signature of cycloether identity, (iv) how the dynamic heterogeneity (DH) behaves as the solution composition passes through the structural stiffening and transition, and (v) whether the time-resolved fluorescence data reflect the signature of the simulated DH.

II. EXPERIMENTAL DETAILS

A. Sample preparation

Laser grade C153 were purchased from Exciton and was used as received. Dioxane and THF (spectroscopic grade)

were obtained from Sigma–Aldrich. Deionized (Millipore) water was used for preparing aqueous solutions of THF and dioxane. Same method was followed to prepare composition dependent THF/water and Diox/water solutions as described in the literature.[34]

B. Steady-state and time-resolved spectroscopic measurements

Absorption spectra of temperature equilibrated (Julabo) aqueous THF and Diox solutions were recorded using UV–Visible spectrophotometer (Model UV–2450, Shimadzu). The emission spectra were recorded (SPEX Fluoromax–3, Jobin–Yvon, Horiba) after adjusting the absorbance of the solutions ~0.1 with excitation wavelength fixed at 409 nm. The slit width for both absorption and emission spectrophotometer was fixed to 2 nm. The spectra were then analysed by the standard procedure[42–46] to obtain the spectral frequencies and full widths at half maxima (FWHMs).

Time resolved fluorescence anisotropy decays were collected using time-correlated single photon counting (TCSPC) technique based on a laser system (Lifespec–ps, Edinburgh, UK) with 409 nm light as excitation. The full width at half maximum of the instrument response function (IRF) with the above excitation was approximately 90 ps. Following the standard method,[47–50] the emission intensity decays of C153 at different THF and Diox concentrations corresponding to emission polarizer orientation at magic angle (54.7°), parallel (0°) $I_{\parallel}(t)$, and perpendicular (90°) $I_{\perp}(t)$ were collected for constructing the composition dependent dynamic fluorescence anisotropy decay, r (t), as follows:

$$r(t) = \frac{I_{\parallel}(t) - GI_{\perp}(t)}{I_{\parallel}(t) + 2GI_{\perp}(t)}. \quad (1)$$

The geometric factor (G) in $r(t)$ was determined via tail-matching and found to be 1.15 ± 0.1.

C. Model and force field

The present simulation study employed SPC/E (extended simple point charge) model of water.[51] For THF, total potential energy function used was of the following form:[52]

$$U = \left[\sum_{bonds} k_r^{ab}\left(r_{ij} - r_0^{ab}\right)^2\right] + \left[\sum_{angles}\left\{k_\theta^{abc}\left(\theta_{ijk} - \theta_0^{abc}\right)^2 - k_r^{ac}\left(r_{ik} - r_0^{ac}\right)^2\right\}\right] + \left[\sum_{torsions}\sum_{n} k_{\tau,n}^{abcd}\left[1 + \cos\left(n\tau_{ijkl} - \tau_0^{abcd}\right)\right]\right] + \left[\sum_{i<j}\left\{4\varepsilon^{ab}\left[\left(\frac{\sigma^{ab}}{r_{ij}}\right)^{12} - \left(\frac{\sigma^{ab}}{r_{ij}}\right)^{6}\right] + \frac{q^a q^b}{4\pi\varepsilon_0 r_{ij}}\right\}\right]. \quad (2)$$

Here, the intramolecular bonded interactions consist of harmonic terms for bond stretching (bond length, r_{ij}, equilibrium bond length, r_0, and bond force constant, k_r), angle bending (bond angle, θ_{ijk}, equilibrium bond angle, θ_0, and angle force constant, k_θ), and torsional potential defined over cosines of the dihedral angle τ_{ijkl} (multiplicity,

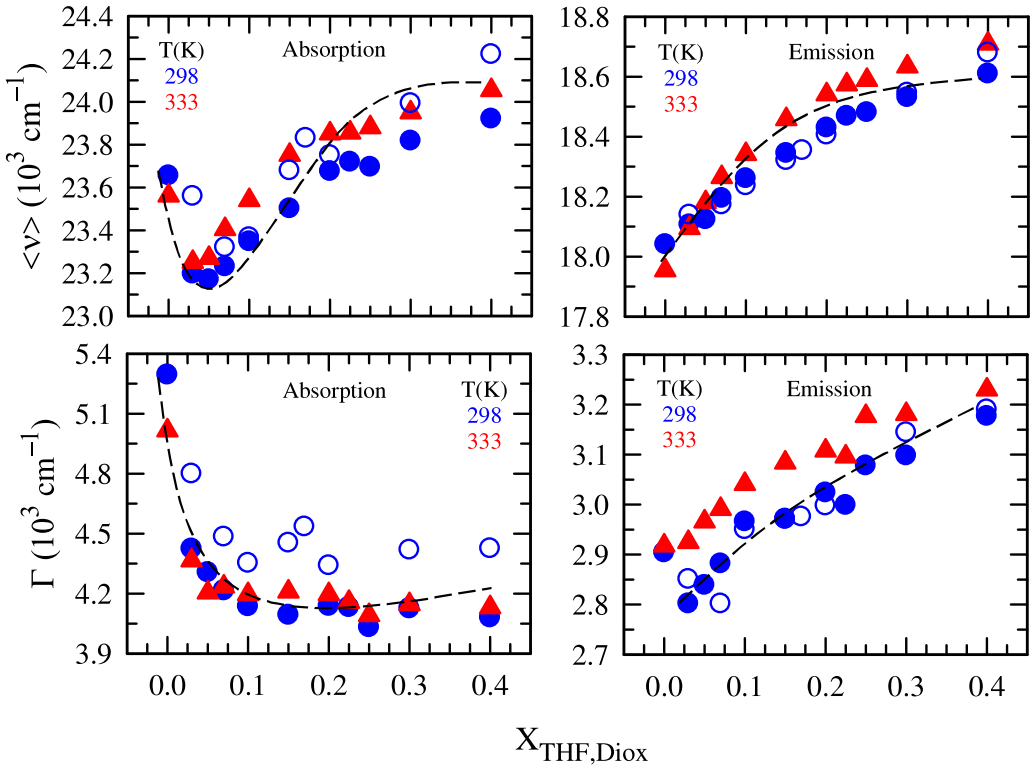

FIG. 1. Cycloether mole fraction (X_{ether}) dependence of absorption (left panels) and emission (right panels) spectral frequencies (ν) and widths (Γ) of C153 at temperatures ~298 K (blue circles) and ~333 K (red triangles). Filled and open symbols represent data in THF/water and Diox/water binary mixtures, respectively. Here, ν is the mean of first moment, peak, and half average frequencies, Γ the FWHM. Dashed lines are guides to the bare eyes. Uncertainties associated with $\langle\nu\rangle$ and Γ are typically ±200 cm^{-1} and ±100 cm^{-1}.

n, phase, τ_0, and torsional parameter, $k_{\tau,n}$). The two-body Urey–Bradley 1–3 interaction term is also included here which comprises a harmonic potential along the distance between first and third atoms of a bond angle. The nonbonded interactions were included by Lennard–Jones (LJ) and Coulomb interactions. Potential well depth, van der Waals radius, distance between atoms in the above equation are symbolized by ε,σ, and r, respectively. The parameter q represents the partial charge of the atom and ε_0 represents the static dielectric constant. LJ interactions between unlike atoms were calculated via Lorentz–Berthelot combining rule.[53] The force field parameters for THF were taken from CHARMM[52] force field using DL_FIELD.[54]

For Diox, the following form for the potential energy function was considered:[55]

$$U = \left[\sum_{bonds} k_r^{ab}\left(r_{ij} - r_0^{ab}\right)^2\right] + \left[\sum_{angles} k_\theta^{abc}\left(\theta_{ijk} - \theta_0^{abc}\right)^2\right] + \left[\sum_{torsions}\left\{\frac{V_1}{2}(1+\cos\phi) + \frac{V_2}{2}(1-\cos 2\phi) + \frac{V_3}{2}(1+\cos 3\phi)\right\}\right] + \left[\sum_{i<j}\left\{4\varepsilon^{ab}\left[\left(\frac{\sigma^{ab}}{r_{ij}}\right)^{12} - \left(\frac{\sigma^{ab}}{r_{ij}}\right)^{6}\right] + \frac{q^a q^b}{4\pi\varepsilon_0 r_{ij}}\right\}\right]. \quad (3)$$

Except V_1, V_2, V_3 which are the coefficients of the Fourier series and ϕ (the torsion angle), all other parameters have usual meaning as described above. The force field parameters and initial coordinates for Diox and C153 were adopted from the relevant literatures.[55,56] Note that all the bond lengths of Diox molecules were kept constrained and rigid model[56] of C153 was used in our study. Partial charges for all the atomic sites of C153 were taken from the literature.[56]

D. Simulation details

Simulations at various compositions were carried out with a total number of 512 (cycloether + water) molecules using DL_POLY_Classic suite,[57] employing cubic box with periodic boundary condition.[53] Additionally, one C153 molecule was added into the binary mixtures to maintain a very low solute concentration in the solution. Equations of motions were solved by Verlet–Leapfrog algorithm[53] with time step of 1 fs. Trajectory was obtained running the simulation in canonical (NVT) ensemble using Nosé–Hoover thermostat[58,59] with relaxation time of 0.5 ps at 300 K after reproducing the experimental density in simulation (within ± 2% of experimental density) employing NPT ensemble. For analysis, 4 ns trajectory was saved after 1 ns equilibration. Ewald summation technique[53] and SHAKE algorithm[60] were, respectively, used to handle electrostatic interactions and constrained all bonds involving hydrogen atoms.

III. RESULTS AND DISCUSSION

A. Steady-state studies: Change in spectral behaviour

The change with X_{THF} of steady-state absorption and emission frequency, ν, and width, Γ (full width at half

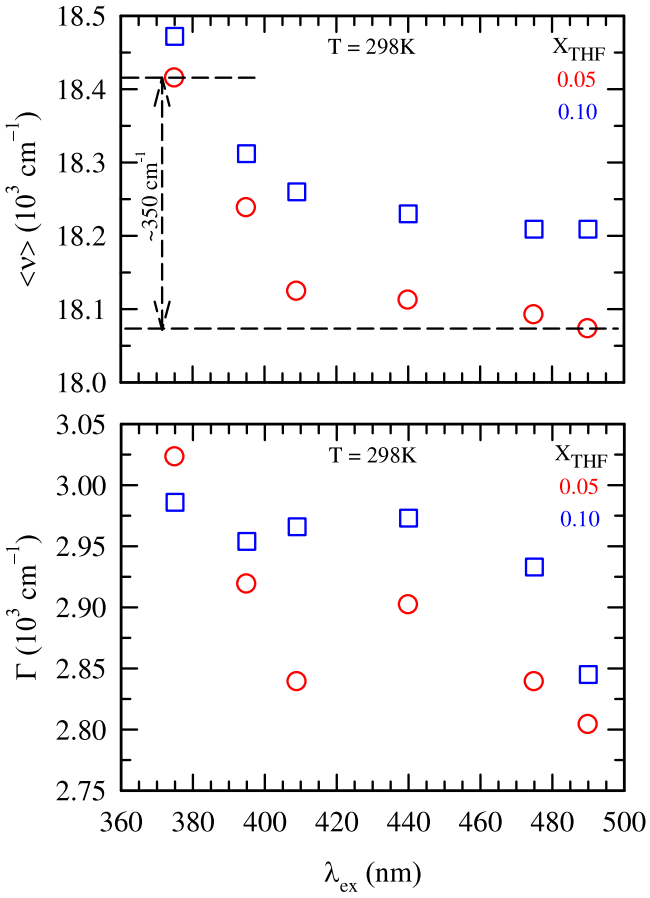

FIG. 2. $\lambda_{ex.}$-dependent emission frequency, ν and FWHM, Γ of C153 in THF concentrations, $X_{THF} = 0.05$ and $X_{THF} = 0.10$ at ~298 K. Note that the largest total absorption red-shift was observed at $X_{THF} = 0.05$. Moderate $\lambda_{ex.}$-dependent emission shift (~350 cm^{-1} at $X_{THF} = 0.05$ and ~300 cm^{-1} at $X_{THF} = 0.10$) signifies aggregation in aqueous solutions at low cycloether concentrations. Uncertainties associated with $\langle\nu\rangle$ and Γ are the same as indicated in the caption of Fig. 1.

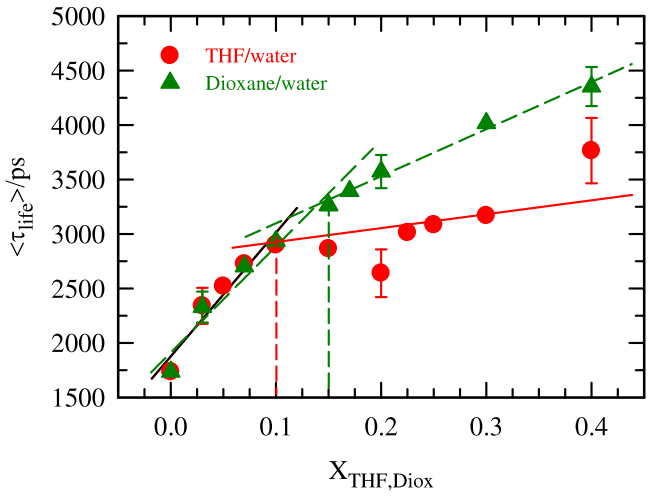

FIG. 3. Variation of the measured average excited-state lifetime, $\langle\tau_{life}\rangle$ of C153 dissolved in aqueous solutions of THF (red circles) and dioxane (green triangles). Solid lines through the data show two different slopes. Vertical dashed lines indicate the cycloether concentrations where changes in the respective slopes have taken place.

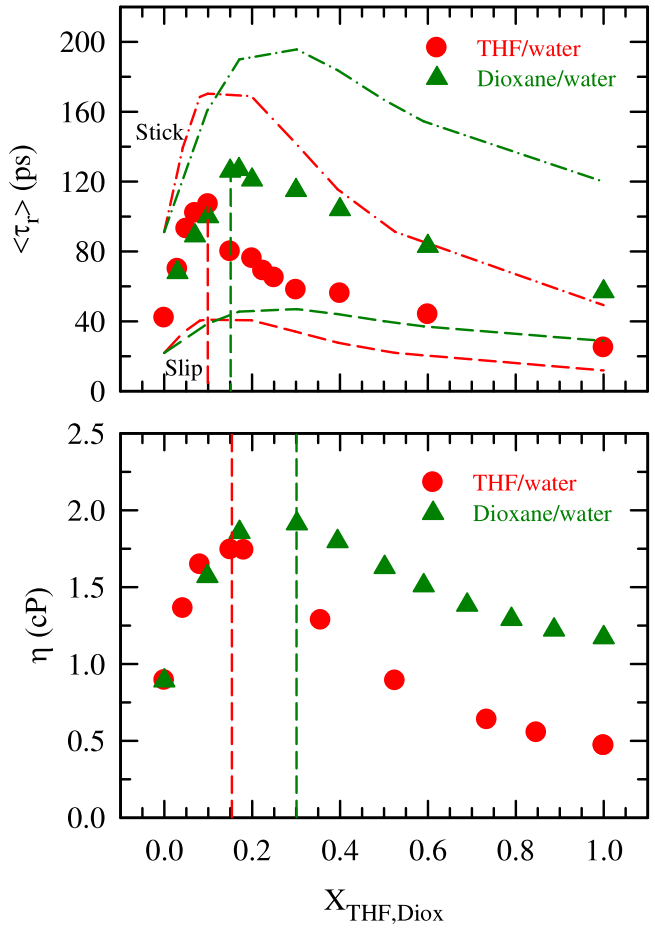

FIG. 4. X_{ether}-dependence of the measured average rotational time, $\langle\tau_r\rangle$ of C153 (upper panel) and viscosity ceofficient, η (lower panel) in THF/water (red circles) and dioxane/water (green triangles) mixtures at ~298 K. Predicted $\langle\tau_r\rangle$ of C153 from the SED relation using stick (dashed-dotted lines) and slip (dashed lines) boundary conditions are shown in the upper panel. Vertical dashed lines represent the composition of cycloethers where structural transition is believed to have taken place. Uncertainties in the measurement of $\langle\tau_r\rangle$ are within ±5% of the reported values.

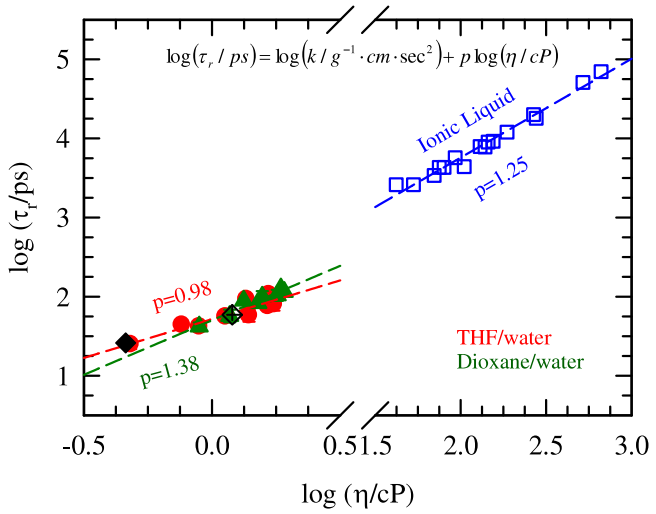

FIG. 5. Viscosity dependence of average rotational time, $\langle\tau_r\rangle$ of C153 in THF/water (red circles) and dioxane/water (green triangles) mixtures. Error bars for few representative cycloether mole fractions are shown. For comparison, $\langle\tau_r\rangle$ of C153 in ionic liquids[67] (blue squares) are also plotted in the figure. Linear fits to the data by the equation given in the inset of the figure are shown by the broken lines. p values obtained from the fit are shown in the figure. Data for $\langle\tau_r\rangle$ of C153 in pure THF and dioxane taken for the literature[47] are represented in the figure by the filled and crossed black diamond symbols, respectively.

maximum), of C153 at two different temperatures, 298 K and 333 K (closer to T_L^C), is shown in Figure 1. Representative steady-state absorption and emission spectra of C153 at 298 K are shown in Figure S1 of the supplementary material.[61] Note that absorption frequency undergoes an initial decrease and records a red-shift of ~550 cm^{-1} at X_{THF} = 0.05, and then further addition of THF reverses the slope producing the expected blue-shift of ~750 cm^{-1} at 298 K as the mixture composition reaches to X_{THF} = 0.40. As observed before in aqueous binary mixtures of tertiary butanol (TBA) and 2-BE (TBA/water[45,46] and BE/water[34] systems), this initial red-shift contradicts the composition dependent solution density,[62] polarity,[63,64] and refractive index[63] depicted in Figure S2 (supplementary material).[61] Furthermore, this concentration is far from critical concentration of THF/water mixture,[2] X_{THF}^C = 0.225. The initial red-shift therefore suggests enhancement of the local solvation structure around C153 which may occur, as in the cases for alcohol-water mixtures,[34,45,46] due to the cosolvent-induced stiffening of the H-bond network of water rather than from the solution criticality effects. Almost comparable amount of red-shift followed by blue-shift is also observed in Diox/water binary mixtures which does not show any solution criticality[3] around room temperature. Absorption spectral widths also report anomalous composition dependence at low mole fraction as they report significant narrowing while undergoing red-shift. However, emission spectral widths follow the ambient neat liquid behaviour.[65] Widths at 333 K show the same trend. All these observation may therefore suggest that the solution criticality does not play any role in producing the anomalous absorption spectral characteristics at low cosolvent concentrations in these aqueous binary mixtures; it is the cosolvent-induced modification in the water structure that provides an unique local solvation shell, producing the absorption red-shift with concomitant narrowing at the low cycloether mole fraction regime.

The above is further supported by the fact that the total absorption red-shift at 333 K is less (~300 cm^{-1}) than that at 298 K (see Figure 1) although this temperature (333 K) is closer to the critical temperature (T_L^C = 344 K). This reflects softening of the cosolvent-water H-bond interaction and randomization of solution structure at higher temperature. Interestingly, corresponding emission frequencies of C153 do not exhibit any cosolvent concentration dependent anomaly, reporting only the change expected based on solution polarity or field factor.[1] This we interpret, as in the cases for alcohol/water mixtures, in terms of excited solute sensing only the averaged-out solvation environment due to a large number of rapid fluctuations during its excited-state lifetime (~2–5 ns).

In Figure 2, we have further investigated excitation wavelength ($\lambda_{ex.}$) dependent emission of C153 at X_{THF} = 0.05 where the maximum red-shift in absorption frequency has been observed and at X_{THF} = 0.10 where absorption frequency started to register usual spectral behaviour. If

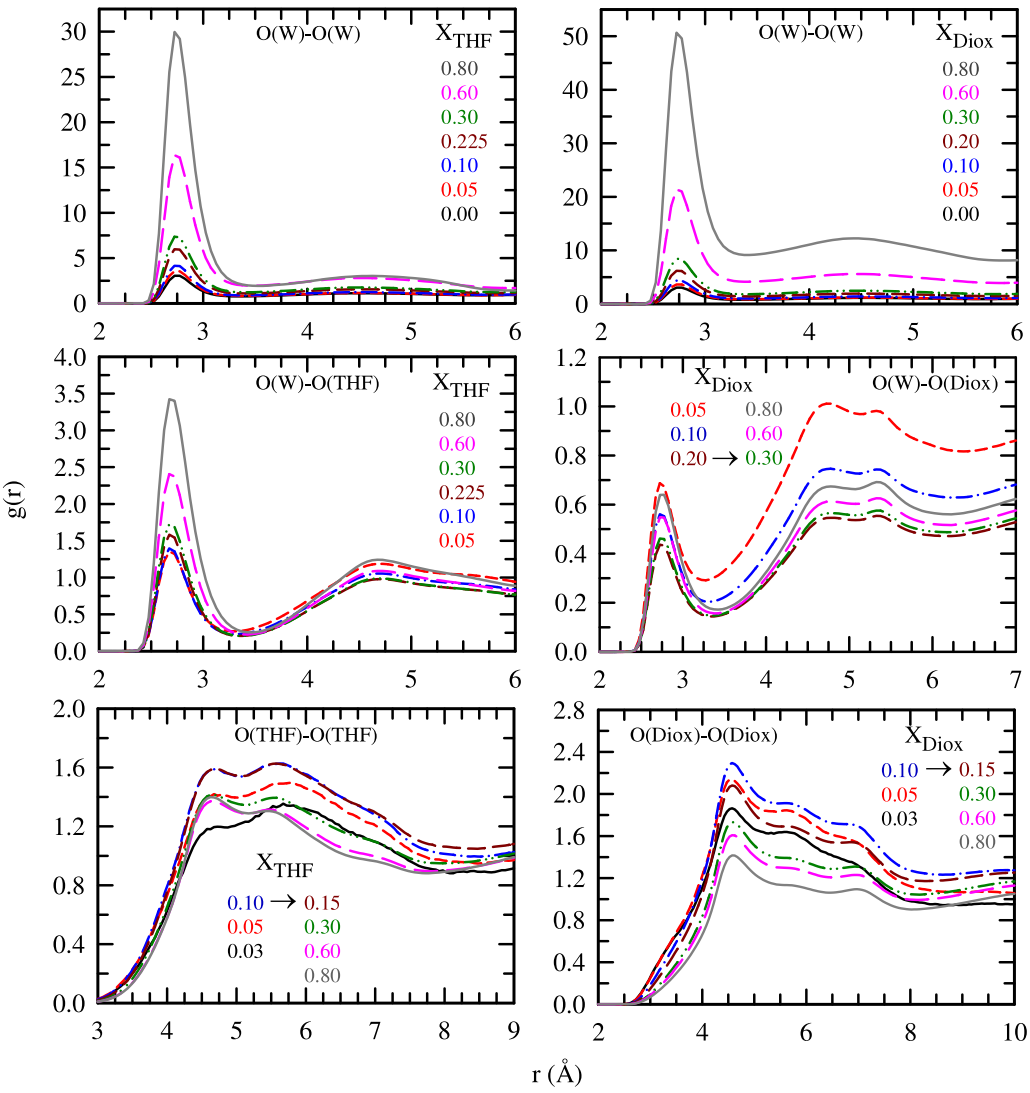

FIG. 6. Simulated radial distribution function (RDF), $g(r)$ between several atomic pairs as a function of distance r for binary mixtures of THF/water (left panels) and dioxane/water (right panels). Atomic pairs are indicated in the inset of every panel. Cycloether compositions are colour-coded. Colour codes are as following: neat water/0.03: black solid line, 0.05: red short-dashed, 0.10: blue dashed-dotted, 0.15/0.225/0.20: dark red medium-dashed, 0.30: green dashed-dotted-dotted, 0.60: pink large-dashed, 0.80: gray solid line. Arrow in each panel indicates the concentration at which RDF changes its peak intensity.

there exists some aggregated structures with sufficiently longer time scales, emission frequency will show $\lambda_{ex.}$ dependence as was observed before for BE/water mixtures at low BE concentrations.[34] Here, we found $\lambda_{ex.}$ dependent emission frequency shift $\Delta\nu_{em}(\lambda_{ex.}) = \nu_{em}(\lambda = 375\ \text{nm}) - \nu_{em}(\lambda = 490\ \text{nm}) = 340\text{cm}^{-1}$ at $X_{THF} = 0.05$ and $280\ \text{cm}^{-1}$ at $X_{THF} = 0.10$. Such values of $\lambda_{ex.}$ dependent emission shifts indicate heterogeneity in solution structure. This solution heterogeneity at low cycloether concentration may originate either via formation of water-cycloether clusters or via hydrophobicity-induced aggregation of cycloether molecules. Whatever be the reasons, it is evident that these spatially heterogeneous structures are longer-lived because they are detectable in the fluorescence measurements.

We would like to mention here that dynamic light scattering measurements[31] of THF/water binary mixtures have revealed that the concentration fluctuation correlation length at critical concentration $X^C_{THF} = 0.225$ grows as one approaches the LCST (344 K). Therefore, it is important to check whether the temperature-dependent absorption spectral response at X^C_{THF} reflect any signature of the concentration fluctuations. We have shown in Figure S3 (supplementary material)[61] the change of absorption frequency and width of C153 with temperature at $X^C_{THF} = 0.225$ which reports blue-shift with temperature (because of the consequent decrease in solution polarity) accompanied by spectral broadening. Such behaviour with temperature for absorption spectrum of C153 is normal.[65]

B. Time-resolved studies: Fluorescence lifetime and rotational time of C153 in the binary mixtures

Average fluorescence lifetime, $\langle\tau_{life}\rangle$ of C153 has been obtained from bi-exponential and single-exponential fitting of the magic angle fluorescence emission decays in THF/water and Diox/water, respectively. The fit parameters are summarized in Tables S4 and S5 of the supplementary material.[61] Figure 3 shows the composition dependence of $\langle\tau_{life}\rangle$ for both THF/water and Diox/water binary mixtures.

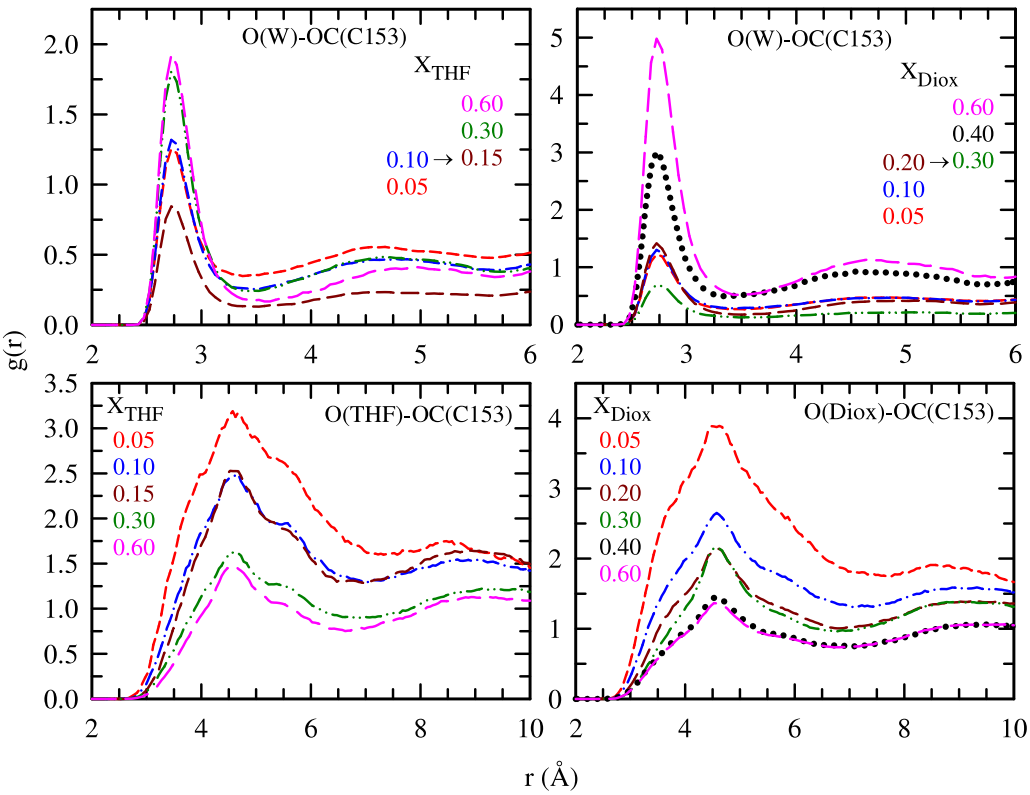

FIG. 7. Plot of simulated RDF, $g(r)$ as a function of distance, r corresponding to the interaction of C153 with the hydrophilic moieties of water and cycloethers in THF/water (left panels) and dioxane/water (right panels) systems. Cycloether compositions are colour-coded and indicated in each panel. Atomic pairs are shown in the inset of the panels.

The X_{ether}-dependent variation of $\langle\tau_{life}\rangle$ produces two distinctly different slopes which intersect, respectively, at $X_{THF} \sim 0.10$ and $X_{Diox} \sim 0.15$. This strongly suggests that solution structures in these binary mixtures undergo transitions at these respective compositions. Note these cycloether concentrations are higher than the compositions at which the maximum absorption red-shift ($X_{ether} \sim 0.05$) occurred due to cosolvent-induced stiffening of water H-bond network structure.

Rotational anisotropy, $r(t)$, of C153 in these binary mixtures have been constructed from fluorescence emission decays using Equation (1). Representative $r(t)$ decay and exponential fit to the experimental data for $X_{THF} = 0.07$ is shown in Figure S6 (supplementary material).[61] Fit parameters at the THF and Diox concentrations are tabulated in Tables S7 and S8 of supplementary material.[61] Single exponential function was required for adequate fitting at lower X_{THF} and pure components whereas bi-exponential function was required for all other X_{ether}. Average rotational time, $\langle\tau_r\rangle$ of C153 is shown as a function of X_{ether} in the upper panel of Figure 4. τ_r values predicted via Stokes–Einstein–Debye (SED) relation[47] for both stick and slip boundary conditions at different cycloether concentrations are also shown in the same figure. Experimental composition dependent viscosity coefficients (η) for both THF/water[66] and Diox/water[62] binary mixtures are also provided in the same figure (lower panel). Clearly, $\langle\tau_r\rangle$ slows down at the lower cycloether concentrations in these aqueous mixtures. There are maxima for $\langle\tau_r\rangle$ at $X_{THF} = 0.10$ and $X_{Diox} = 0.15$ for THF/water and Diox/water binary mixtures, respectively. After the maxima, $\langle\tau_r\rangle$ gradually decrease with further increase of cycloether concentrations in water. Viscosity in these media also passes through a maximum, which appears at $X_{THF} = 0.15$ and $X_{Diox} = 0.30$ for THF/water and Diox/water binary mixtures, respectively. Slope change in $\langle\tau_r\rangle$ at composition lower than the composition of viscosity-maximum therefore suggests a critical role played by solution structure in regulating the rotational motion of a dissolved solute. Note also these solution compositions are different from those where the maxima in absorption red-shift were observed. However, these are the same cosolvent (cycloether) concentrations where slope changes in $\langle\tau_{life}\rangle$ also occurred. In case of alcohol/water binary mixtures[34,46] we have seen that there were two different alcohol concentration regimes where H-bond strengthening/stiffening (relatively lower concentration) and structural transition (relatively higher concentration) took place. In the present scenario, the increase of $\langle\tau_r\rangle$ at low cycloether concentrations reflects increased friction due to a stiffening of water structure. This agrees well with the observation from other studies[12–15] such as light scattering, SANS, NMR that water–cycloether interaction enhances in the intermediate cycloether concentration regime $0.10 \leq X_{Cyet} \leq 0.20$. Further addition of cosolvent beyond this composition leads to structural loosening due to the disruption of three-dimensional H-bond network of water, allowing the solute to rotate relatively freely. As a result, solute rotation time becomes faster with further increase of cycloether in the mixture. Note also in this figure that measured $\langle\tau_r\rangle$ in both these binary mixtures lie in between the SED slip and stick predictions. This further indicates an important role for the solution structure on the rotation of a dissolved solute.

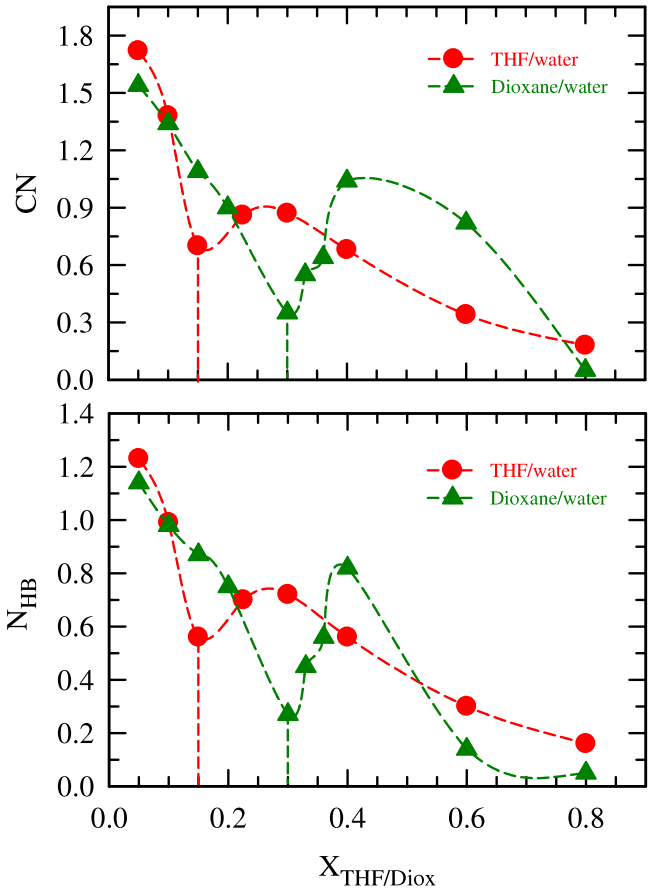

FIG. 8. Simulated number of water molecules (CN) in the first solvation shell of OC group of C153 [Scheme 1] (upper panel) and number of H-bonds (N_{HB}) between OC group and water molecules (lower panel) as a function of X_{ether} in THF/water (red circles) and dioxane/water (green triangles) systems.

Next, we investigate the viscosity coupling of solute rotation in Figure 5 where the measured rotational times of C153 in these binary mixtures are shown as a function of solution viscosity. Linear fits of the binary mixture data (equation given in the inset) reflect a hydrodynamic viscosity dependence for C153 rotation in THF/water mixtures (p = 0.98) but a considerable deviation from such a hydrodynamic dependence for Diox/water mixtures (p = 1.38). Interestingly, C153 rotation times in ionic liquids (ILs),[67] shown in the same figure, also reflect a behaviour similar to that in Diox/water mixtures although these systems (ILs and Diox/water mixtures) differ greatly in interactions and chemical structures. The similarity in the viscosity dependence of rotation times in these two widely different systems, therefore, confirms again that solvent frictional coupling depends both on solution structure[47] and packing (around the rotating solute).[68,69]

C. Solution structure: Insight from simulated radial distribution functions (RDFs)

1. Cycloether-water interaction

Site–site radial distribution functions, $g(r)$, between different atomic pairs of water and cycloethers (in the absence of C153) are shown as a function of distance, r in Figure 6. Note the wide difference in the intensity scale between the water-water RDF and the other RDFs presented here. Clearly, the first peak intensity of the RDF between the oxygen atoms of water, O(W)–O(W) (upper panels), increases with the increase of cycloether concentration for both THF/water and Diox/water binary mixtures. Interestingly, this growth at low concentrations is nearly independent of the cycloether identity (see Figure S9, supplementary material).[61] However, at higher concentrations, O(W)–O(W) RDF senses the cycloether identity and, at 0.8 mole fraction, the first peak of $g(r)$ for Diox/water system becomes nearly double than that for THF/water system. All these features of O(W)–O(W) indicate cycloether-induced stronger (relative to neat water) water-water interaction in these binary mixtures. Interestingly, O(W)–O(ether) RDF shows complex concentration dependence: for THF/water mixtures, the first peak intensity increases with increasing THF mole fraction whereas the O(W)–O(Diox) RDF shows initial decrease up to $X_{Diox} = 0.20$ and then increases with X_{Diox}.

Lower panel shows the RDF between cycloether O atoms, O(ether)–O(ether). Note that there was no peak at the distance of collision diameter of the oxygen atom. This suggests the nonexistence of the first solvation shell around the cycloether O atoms in both these binary mixtures. This is probably due to the closed loop structure of the cycloethers which prevents packing of cycloether molecules at the distance of collision diameter of the oxygen atom. RDF peak intensity of the second solvation shell shows non-monotonic composition dependence for both the binary mixtures. It grows up to $X_{ether} = 0.10$, then decreases with the increase of X_{ether}. Interestingly, this is the mixture composition around which abrupt change in slopes for the measured composition dependent $\langle\tau_{life}\rangle$ and $\langle\tau_r\rangle$ has been observed. Similar composition dependence can also be found for the carbon-carbon RDF among the cycloether molecules in these aqueous mixtures (see Figure S10 of the supplementary material).[61]

2. Interaction of C153 with cycloether and water in binary mixtures

We have chosen carbonyl oxygen (OC, polar moiety) of C153 (shown in Scheme 1) in order to follow how polar interaction between C153 and oxygen atoms of water and cycloether molecules drives the solvation structure around C153. The role of non-polar interaction between C153 and cycloether is then investigated via following the interaction of the ring carbon atoms C2 and C4 of C153 with carbon atoms of cycloethers. Interaction of polar moieties of C153 with the binary solvents is shown in Figure 7 which suggests preferential interaction with water than cycloether, although C153 contains a large non-polar (hydrophobic) moiety. Here again reversal of simulated water-C153 RDF intensities occurs around the cycloether concentrations (see upper panel) at which the measured time scales suggested structural modification via slope-changes. After this composition, g(r) peak intensity of O(W)–OC(C153) increases with increase of X_{ether} (upper panel). In contrast, the O(ether)–OC(C153) RDF peak intensity (shown in the lower panel) decreases with the

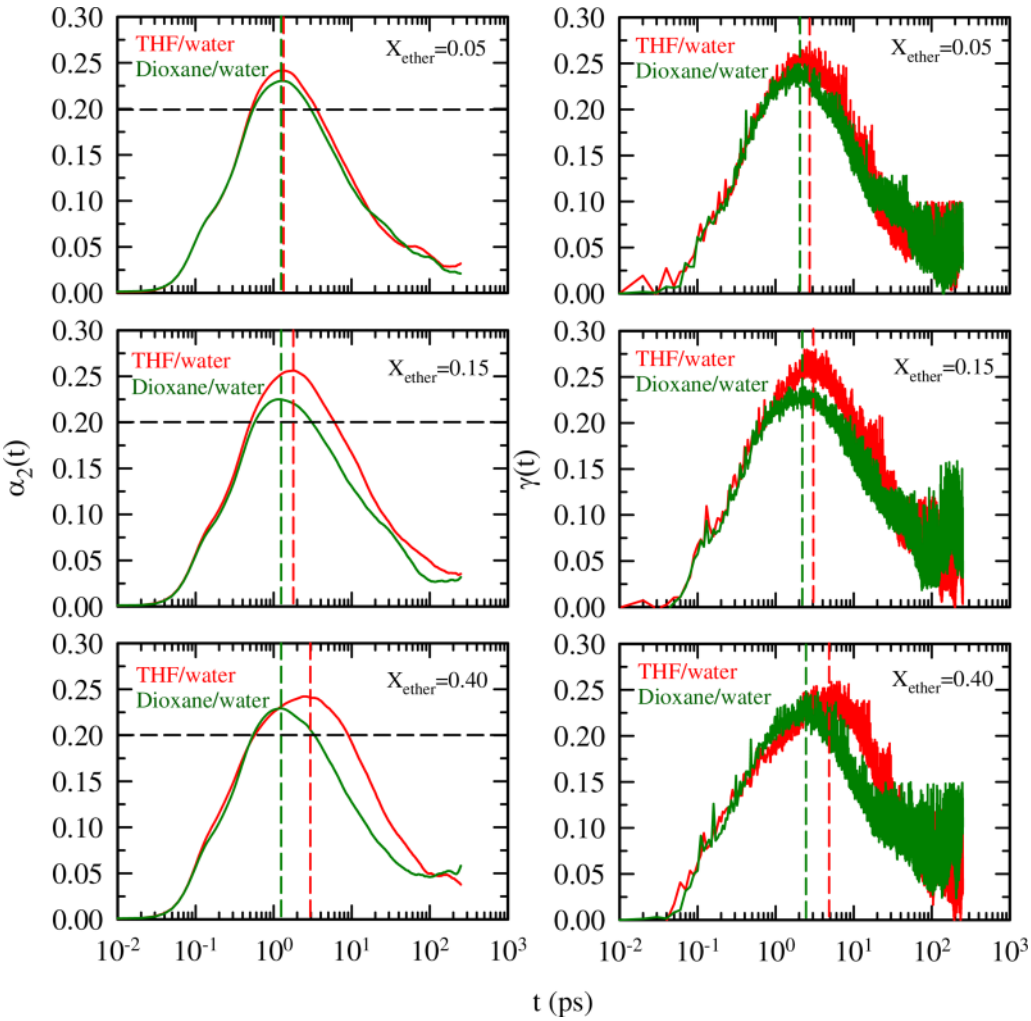

FIG. 9. Simulated $\alpha_2(t)$ (left panels) and $\gamma(t)$ (right panels) for water in THF/water (red colour) and dioxane/water (green colour) mixtures at ~300 K. Cycloether mole fractions (X_{ether}) are shown in each panel. Vertical lines indicate peak times τ_{NG} and τ_{NNG} of $\alpha_2(t)$ and $\gamma(t)$, respectively. Horizontal lines represent peak value of $\alpha_2(t)$ for homogeneous liquids.

increase of X_{ether}. Identical behaviour is also observed for C(ether)–C2(C153) and C(ether)–C4(C153) RDFs shown in Figure S11 (supplementary material).[61]

As C153 interacts preferentially with water in these binary mixtures, we have further calculated the number of water molecules in the first solvation shell of OC site of C153 by using the formula[70]

$$CN = \int_0^R \rho_\beta g_{\alpha-\beta}(r)\, 4\pi r^2 dr, \tag{4}$$

where CN denotes the coordination number of water molecules and R the first minimum distance of the $g(r)$ which is 3.5 Å in the present case. ρ_β is the number density of water. CN calculated thus are shown in the upper panel of Figure 8. Note CN of water decreases with increasing cycloether concentration at this water-rich regime for both the binary mixtures. This means release of water molecules to the bulk during the process of structural transition which is supported by the increase in solution entropy. Interestingly, CN shows minima at $X_{THF} = 0.15$ and $X_{Diox} = 0.30$ around which measured $\langle\tau_{life}\rangle$ and $\langle\tau_r\rangle$ also exhibit abrupt changes in slope. After this, CN continues to increase up to $X_{THF} = 0.30$ and $X_{Diox} = 0.40$ because the solution structure supports increased interaction between water and C153 in these aqueous solutions. Increase of cycloether concentration beyond these mole fractions leads the solutions to the water-depleted regime where CN (of water) naturally decreases. We have further calculated the number of H-bonds (N_{HB}) OC can form with water molecules using the following geometric conditions between the donor and the acceptor:[71,72] (i) the donor-acceptor O–O distance must be less than 3.5 Å, (ii) the angle between O–O bond vector and O–H bond vector must be less than 30°, and (iii) the O–H distance of donor-acceptor must be less than 2.45 Å. The distance criteria correspond to the first minimum of the respective RDFs. The results are shown in the lower panel of Figure 8. Distribution of N_{HB} with cycloether concentration also produces the similar pattern as observed for the composition dependent CN. These two simulated parameters, CN and N_{HB}, therefore, provide a microscopic view of the solution structural transition suggested by the dynamic fluorescence anisotropy and lifetime measurements.

Because solution structure is intimately related to the DH,[73,74] we next explore the composition dependence of several DH parameters that may be useful in understanding

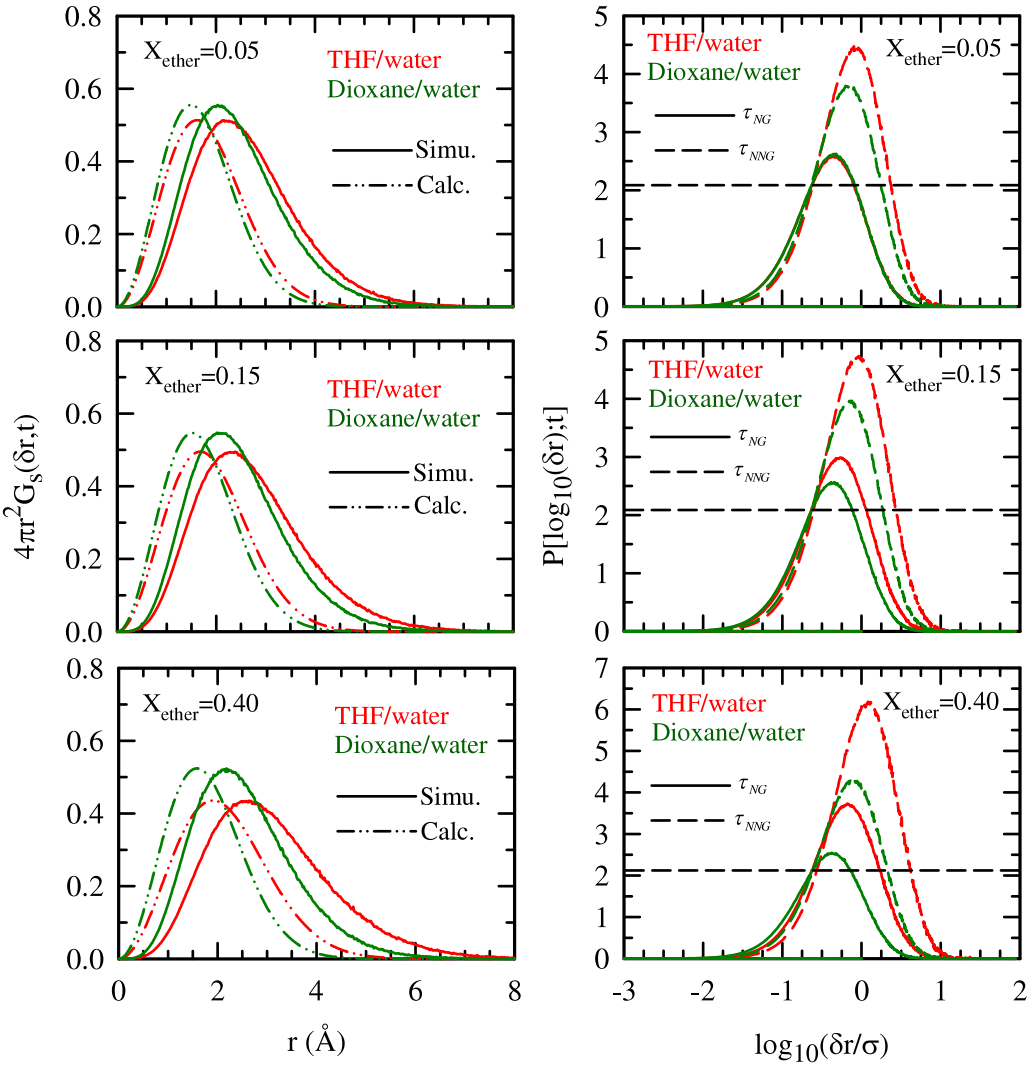

FIG. 10. Self part of the van Hove time correlation function, $G_s(\delta r,t)$ (left panels), and simulated single particle distribution function, $P[\log_{10}(\delta r);t]$, for water in THF/water (red) and Diox/water (green) mixtures at ~300 K. Cycloether mole fractions (X_{ether}) are shown in each panel. $G_s(\delta r,t)$ obtained from simulations and Gaussian approximation are represented by solid and broken lines, respectively. While $P[\log_{10}(\delta r);t]$ are shown here at peak times τ_{NG} (solid lines) and τ_{NNG} (dashed lines), respectively, $G_s(\delta r,t)$ are shown only at τ_{NNG} to avoid clutter. Horizontal lines in the right panels indicate the value of $P[\log_{10}(\delta r);t]$ for a Gaussian $G_s(\delta r,t)$.

the dynamical response of these binary mixtures. In addition, qualitative idea about the growth of the correlation length with composition suggesting formation of domains or clusters may also be generated. This may help in understanding the structural heterogeneity aspect of these solutions.

D. Solution dynamic heterogeneity: Mixture composition dependence

1. Non-Gaussian and new non-Gaussian parameters

A primary test for the presence of DH (that is, spatially varying relaxation rates) can be conducted by following the time dependence of the non-Gaussian (NG) parameter as follows:[74–77]

$$\alpha_2(t) = \frac{3\langle \Delta r^4(t)\rangle}{5\langle \Delta r^2(t)\rangle^2} - 1, \tag{5}$$

where $\Delta \boldsymbol{r}(t) = \boldsymbol{r}_i(t) - \boldsymbol{r}_i(0)$ with Δr denoting the single particle displacement. In complex systems, however, there may exist a time scale slower than suggested by $\alpha_2(t)$, which can be followed via the new non-Gaussian (NNG) parameter, defined as[77–79]

$$\gamma(t) = \frac{1}{3}\langle \Delta r^2(t)\rangle \left\langle \frac{1}{\Delta r^2(t)} \right\rangle - 1. \tag{6}$$

Figure 9 shows $\alpha_2(t)$ and $\gamma(t)$ for water molecules in these binary mixtures at three representative compositions covering the mole fractions at which structural stiffening and transition have been found to occur. These parameters for neat ambient water are shown in Figure S12 (supplementary material).[61] For homogeneous liquids, $\alpha_2(t) \approx 0.2$[75] at the peak-time (τ_{NG}) and this is reflected in Fig. S12 of the supplementary material.[61] Note in Fig. 9 that neither $\alpha_2(t)$ and $\gamma(t)$ for water exhibit any particular dependence on mixture compositions where structural changes (stiffening or transition) occurs; they show only that these mixtures are slightly more dynamically heterogeneous than neat water with α_2 peak time scale (τ_{NG}) ~ 1-3 ps and γ peak time scale (τ_{NNG})~2-5 ps. Also, water molecules in aqueous mixtures

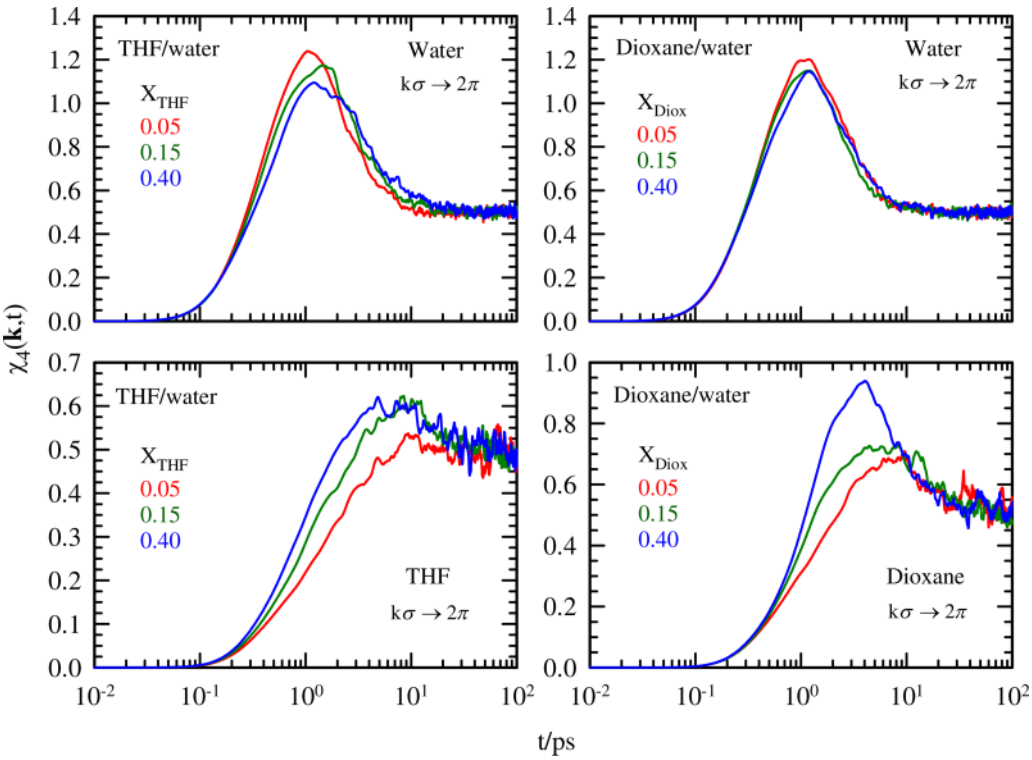

FIG. 11. Four point dynamic susceptibility, $\chi_4(\mathbf{k},t)$, for water (upper panels) and cycloethers (lower panels) in THF/water (left panels) and Diox/water (right panels) mixtures. Cycloether mole fractions (X_{ether}) are colour-coded and shown in each panel. $\chi_4(\mathbf{k},t)$ has been calculated at the nearest neighbor wavenumber, $k\sigma \rightarrow 2\pi$. Here, σ is the distance at which the first maximum of $g(r)$ appears. In the calculations, only oxygen atom(s) of cycloethers are considered to represent the cycloether molecule. The peak time of $\chi_4(\mathbf{k},t)$ is denoted by τ_4^{max}.

of THF show somewhat more dynamical heterogeneity than those in Diox/water mixture with peak time scales slightly longer for THF/water mixtures at these concentrations. Similar NG and NNG features are also predicted for THF and Diox molecules in these aqueous solutions at these compositions (see Fig. S13 of the supplementary material).[61] Interestingly, the τ_{NG} and τ_{NNG} time scales predicted here (see Table S14 of the supplementary material[61]) are quite close to the slow time scales that govern more than 50% of the total solvation energy relaxation in neat ambient THF (~1.5 ps, ~55%) and Diox (2.2 ps, ~52%).[65] Such similarity provides a support to the conjecture that these DH time scales are correlated to the slow solvation rates in these systems.[74]

2. Single particle displacement distribution

Single particle displacement distribution can reveal the DH signatures via its departure from Gaussian distribution predicted for homogeneous systems. This is obtained from the time dependent self part of the van Hove correlation function,[53] $G_s(\delta r,t)$ as follows:[77–79]

$$P[\log_{10}(\delta r);t] = \ln(10)4\pi\delta r^3 G_s(\delta r,t). \quad (7)$$

Figure 10 shows the simulated $G_s(\delta r,t)$ and $P\left[\log_{10}(\delta r);t\right]$ along with the Gaussian distributions for water molecules in THF/water and Diox/water mixtures at the three representative cycloether concentrations. Note the substantial deviation of the simulated $G_s(\delta r,t)$ from the calculated Gaussian behaviour, suggesting that these mixtures are considerably dynamically heterogeneous. In addition, the peaks of these distributions are occurring within ~2-2.5 Å which is larger than that predicted by the corresponding Gaussian distributions. In addition, the peak position shifts slightly to larger lengths with the mixture composition and for aqueous THF mixtures. This lengthscale (~2-2.5 Å) is comparable to water molecular diameter.[80] In addition, the long tail of these distributions extends to a length approximately twice the diameter of a water molecule. All these suggest that water in these binary mixtures access displacements that are considerably larger than those expected for temporally homogeneous systems. For $P\left[\log_{10}(\delta r);t\right]$, deviation from the predicted peak height of ~2.13 for homogeneous systems[78] at both τ_{NG} and τ_{NNG} provides further support to the above DH view. Figure S15 of the supplementary material[61] presents a plot of $P\left[\log_{10}(\delta r);t\right]$ at t = τ_{NG} and τ_{NNG} for neat ambient water, and a comparison clearly demonstrates that water in these binary mixtures are significantly more heterogeneous than in the neat system.

3. Four point dynamic susceptibility, correlation times and lengths

Four point dynamic susceptibility, $\chi_4(\mathbf{k},t)$, which describes how molecular motions at two different space points are correlated over a certain time duration, can be obtained approximately from the fluctuations of the self-intermediate scattering function, $F_s(\mathbf{k},t)$ as follows:[81–83]

$$\chi_4(\mathbf{k},t) = N\left[\left\langle F_s(\mathbf{k},t)^2\right\rangle - \left\langle F_s(\mathbf{k},t)\right\rangle^2\right], \quad (8)$$

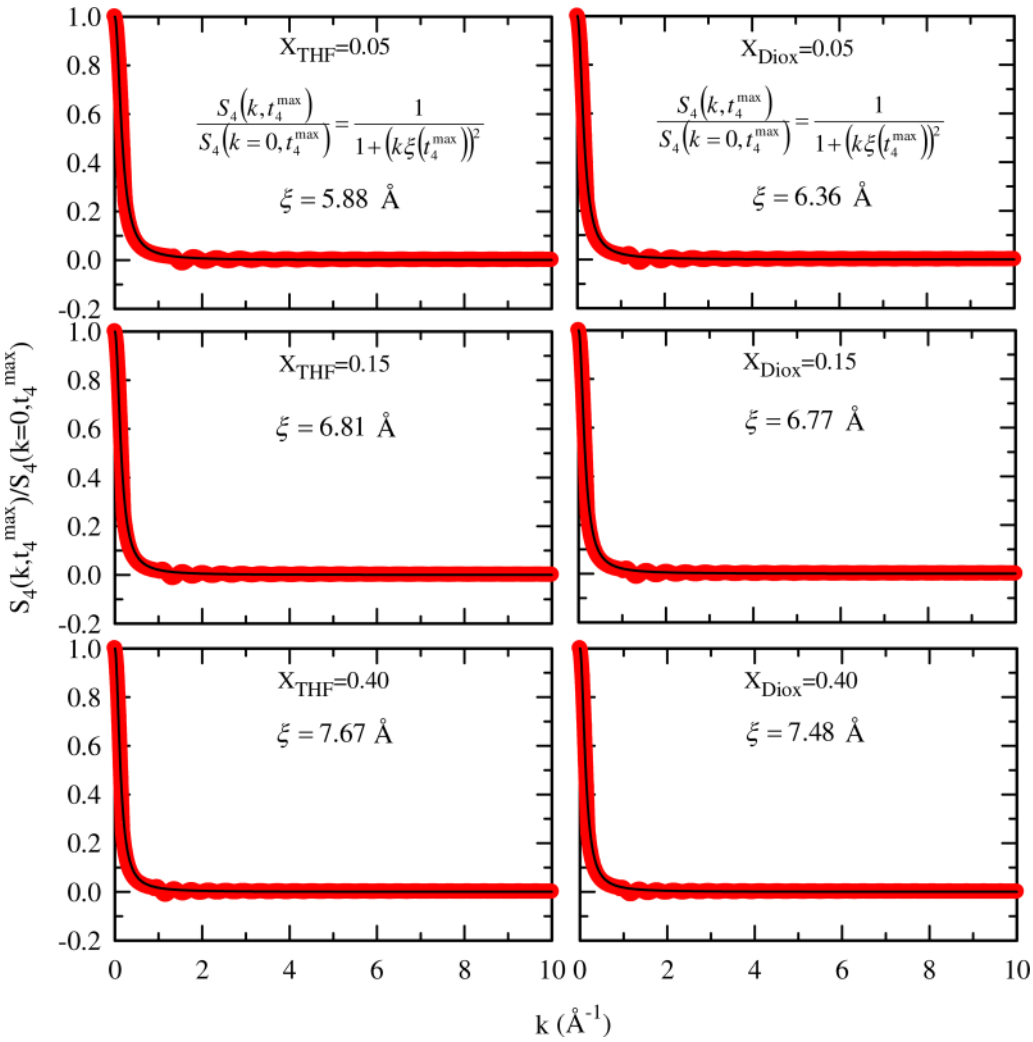

FIG. 12. Estimation of dynamic correlation lengths (ξ) for water at different compositions of THF/water (left panels) and Diox/water (right panels) binary mixtures at ~300 K. Circles represent the simulated data and the lines going through them denote fits using Eq. (10) (shown in the top panel).

where $F_s(\mathbf{k},t) = \frac{1}{N}\sum_{i=1}^{N}\langle\cos\mathbf{k}\cdot[\mathbf{r}_i(t)-\mathbf{r}_i(0)]\rangle$. All the calculations have been carried out for nearest neighbour wavevector, $k\sigma = 2\pi$. σ being the length at which the first peak of the simulated g(r) appears.

This two point density correlation function estimated at the nearest neighbour wavevector, $F_s(\mathbf{k}\sigma \rightarrow 2\pi,t)$, exhibits a very similar behaviour with the overlap function, $Q(t)$, which essentially quantifies the overlap between a configuration at $t = 0$ with a later time t. $Q(t)$ is defined as

$$Q(t) = \sum_{i=1}^{N} w(|\mathbf{r}_i(0) - \mathbf{r}_i(t)|), \tag{9}$$

where $w(|\mathbf{r}_1 - \mathbf{r}_2|)$ is unity if $|\mathbf{r}_1 - \mathbf{r}_2| \leq a$, else zero with $a = 0.3\sigma$ (σ is the diameter of the particle of interest). The simulated decays of $F_s(\mathbf{k}\sigma \rightarrow 2\pi,t)$ and $Q(t)$ for water and cycloether molecules at the three representative compositions for these mixtures are shown in Figure S16 of the supplementary material.[61] The e^{-1} times reflected by these composition dependent decays are within ~1-4 ps (see Table S17 of the supplementary material[61]) which correlate well with the time scales associated with τ_{NG} and τ_{NNG}. This indicates that DH time scales originate from the centre-of-mass relaxation of the particles at the nearest neighbour.

Simulated $\chi_4(\mathbf{k}\sigma \rightarrow 2\pi,t)$ for both water and cycloether molecules presented in Figure 11 shows non-monotonous t-dependence with a peak time (τ_4^{max}) of ~1-2 ps for water and ~5-10 ps for cycloether molecules (see Table S18 of the supplementary material[61]). Such a non-monotonous behaviour of $\chi_4(\mathbf{k},t)$ has already been seen for glass-forming liquids,[84,85] ionic liquids,[74,86] colloidal gels,[87] and poly-dispersed systems.[88,89] The difference in τ_4^{max} values between water and cycloether molecules indicate more extended temporal correlation among cycloether molecules than among water molecules in these binary mixtures. Note also that τ_4^{max} for cycloether molecules is the largest at the lowest composition studied here. This is possibly an indirect evidence favouring aggregation in dilute aqueous solutions and corroborates well with the excitation wavelength dependence of fluorescence emission observed for THF/water mixtures at low concentration (see Fig. 2).

The emergence of different correlation times (τ_4^{max}) for different species then motivates the estimation of the dynamic correlation lengths ξ at τ_4^{max}. This has been done via numerically fitting the simulated $S_4(\mathbf{k},t)$ to the Ornstein-

Zernike relation as follows:[90–93]

$$\frac{S_4(\mathbf{k},t)}{S_4(\mathbf{k}\to 0,t)} = \frac{1}{1+(\mathbf{k}\xi(t))^p}, \tag{10}$$

where $S_4(\mathbf{k},t) = 4\pi\rho\left[\frac{Q(t)}{N}\right]^2 \int_0^r dr r^2 \frac{\mathrm{Sin}\,\mathbf{k}r}{\mathbf{k}r} g(r)$.

Numerical fits as described above and the estimated ξ for water molecules in these binary mixtures at these representative mole fractions ($X_{THF/Diox} = 0.05, 0.15, 0.40$) are shown in Figure 12. Interestingly, the estimated ξ for water molecules in these mixtures covers a range ~6-8 Å, which is ~2-3 times the water molecular diameter. Similar values of ξ for cycloethers have also been obtained when only the oxygen-oxygen interactions were considered. These lengthscales therefore do not suggest growth of long-ranged spatial correlations leading to formation of mesoscopic domains. Note however that this is a very qualitative estimation for the correlation length because Eq. (10) involves structure factor at the collective ($\mathbf{k} \to 0$) limit that can induce strong system size dependence in computer simulations.[81] Such a caveat notwithstanding the estimated correlation lengths may be considered as indicators of local cluster formation. These clusters can then lead to local heterogeneity in solution structure.

IV. CONCLUSION

In summary, THF/water and Diox/water binary mixtures show both stiffening and transition of the three-dimensional H-bond network structure of water with stiffening occurring at cosolvent (THF or Diox) mole fractions lower than those for transitions. Spectroscopic evidences for cycloether aggregation at very dilute concentrations have been found. Moreover, these structural modifications derive no contributions from the solution criticality, suggesting hydrophobic interaction driven structural transition and aggregation in aqueous media. Quite interestingly, no dependence on the chemical nature of these cosolvent molecules (dipolar or quadrupolar) of the anomalous composition dependence of the solution structure has been found. Such an observation provides support to the view that water structure in these binary mixtures, as previously interpreted for aqueous alcohol solutions, is overwhelmingly influenced by the hydrophobic interaction between the cosolvent and water molecules with no role for the solution criticality. Simulated radial distribution functions reflect abrupt changes in distribution intensities at those compositions around which experiments report structural transition. Minima in simulated water coordination number for the dissolved dipolar solute and number of H-bonds at these solution compositions strongly support the view of structural transition and provide microscopic insight into the anomalous composition dependence of the spectral data. Further study exploring the dependence of solution dynamic heterogeneity[74,77,94,95] also did not show any specific dependence on the chemical nature of the cosolvent. Estimated correlation lengths from the simulated four-point dynamic susceptibility suggest formation of local clusters involving water and cycloether molecules. In addition, DH time scales in these mixtures are predicted to be connected to the slow solvation time scales in these aqueous binary mixtures. Probe dependence (cationic, anionic, and neutral) of solvation and rotational dynamics of these mixtures,[96] and correlating the results obtained here to the mixture composition impact reported by other authors on events involving biologically relevant moieties[97–100] and other solutes[101–103] would be worth pursuing in the future.

ACKNOWLEDGMENTS

We thank the anonymous reviewers for their comments and suggestions which helped in improving the quality of the manuscript. S.I. thanks University Grants Commission (UGC), India for a research fellowship. Simulation works presented here are obtained using the computational facilities provided by a TUE-CMS project at the Centre (Grant No. SR/NM/NS-29/2011(G)).

[1]L. Reynolds, J. A. Gardecki, S. J. V. Frankland, M. L. Horng, and M. Maroncelli, J. Phys. Chem. **100**, 10337 (1996).
[2]A. Oleinikova and H. Weingärtner, Chem. Phys. Lett. **319**, 119 (2000).
[3]T. Kouissi, M. Bouanz, and N. Ouerfelli, J. Chem. Eng. Data **54**, 566 (2009).
[4]S. Budvari, *The Merck Index* (Merck and Co., Rahway, NJ, 1989).
[5]D. N. Glew and H. Watts, Can. J. Chem. **51**, 1933 (1973).
[6]H. Nakayama and K. Shinoda, J. Chem. Thermodyn. **3**, 401 (1971).
[7]M. Sakurai, J. Chem. Eng. Data **37**, 492 (1992).
[8]G. N. Malcolm and J. S. Rowlinson, Trans. Faraday Soc. **53**, 921 (1957).
[9]P. Lejček, J. Matouš, J. P. Novák, and J. Pick, J. Chem. Thermodyn. **7**, 927 (1975).
[10]E. K. Baumgartner and G. Atkinson, J. Phys. Chem. **75**, 2336 (1971).
[11]G. Atkinson, S. Ralagopalan, and B. L. Atkinson, J. Phys. Chem. **85**, 733 (1981).
[12]C. Yang, W. Li, and C. Wu, J. Phys. Chem. B **108**, 11866 (2004).
[13]T. Takamuku, A. Nakamizo, M. Tabata, K. Yoshida, T. Yamaguchi, and T. Otomo, J. Mol. Liq. **103**, 143 (2003).
[14]J. Hao, H. Cheng, P. Butler, L. Zhang, and C. C. Han, J. Chem. Phys. **132**, 154902 (2010).
[15]Y. G. Wu, M. Tabata, and T. Takamuku, J. Mol. Liq. **94**, 273 (2001).
[16]Y. Tominaga and S. M. Takeuchi, J. Chem. Phys. **104**, 7377 (1996).
[17]T. Fukasawa, Y. Amo, and Y. Tominaga, J. Chem. Phys. **118**, 6387 (2003).
[18]T. Takamuku, A. Yamaguchi, M. Tabata, N. Nishi, K. Yoshida, H. Wakita, and T. Yamaguchi, J. Mol. Liq. **83**, 163 (1999).
[19]K. Mizuno, S. Imafuji, T. Fujiwara, T. Ohta, and Y. Tamiya, J. Phys. Chem. B **107**, 3972 (2003).
[20]T. Fukasawa, Y. Tominaga, and A. Wakisaka, J. Phys. Chem. A **108**, 59 (2004).
[21]M. Katayama and K. Ozutsumi, J. Solution Chem. **37**, 841 (2008).
[22]S. Schrödle, B. Fischer, H. Helm, and R. Buchner, J. Phys. Chem. A **111**, 2043 (2007).
[23]S. Schrödle, G. Hefter, and R. Buchner, J. Phys. Chem. B **111**, 5946 (2007).
[24]S. Mashimo, N. Miura, T. Umehara, S. Yagihara, and K. Higasi, J. Chem. Phys. **96**, 6358 (1992).
[25]T. Molotsky and D. Huppert, J. Phys. Chem. A **107**, 8449 (2003).
[26]S. Mukherjee, K. Sahu, D. Roy, S. K. Mondal, and K. Bhattacharyya, Chem. Phys. Lett. **384**, 128 (2004).
[27]A. Chandra and B. Bagchi, J. Chem. Phys. **94**, 8367 (1991).
[28]A. Chandra, Chem. Phys. Lett. **235**, 133 (1995).
[29]S. Chowdhuri and A. Chandra, J. Chem. Phys. **123**, 234501 (2005).
[30]R. Gupta and A. Chandra, J. Chem. Phys. **127**, 024503 (2007).
[31]C. M. Sorensen, J. Phys. Chem. **92**, 2367 (1988).
[32]H. E. Stanley, *Introduction to Phase Transitions and Critical Phenomena* (Oxford University Press, New York, 1971).
[33]N. Ito, T. Kato, and T. Fujiyama, Bull. Chem. Soc. Jpn. **54**, 2573 (1981).
[34]S. Indra and R. Biswas, J. Chem. Phys. **142**, 204501 (2015).
[35]M. D. Smith, B. Mostofian, L. Petridis, X. Cheng, and J. C. Smith, J. Phys. Chem. B **120**, 740 (2016).
[36]K. Remerie, J. B. F. N. Engberts, and W. F. V. Gunsteren, Chem. Phys. **101**, 27 (1986).
[37]P. I. Nagy, G. Völgyi, and K. Takács–Novák, J. Phys. Chem. B **112**, 2085 (2008).
[38]L. C. G. Freitas and J. M. M. Cordeiro, J. Mol. Struct.: THEOCHEM **335**, 189 (1995).

[39]I. Brovchenko and B. Guillot, Fluid Phase Equilib. **183**, 311 (2001).
[40]A. Oleinikova, I. Brovchenko, and A. Geiger, J. Chem. Phys. **117**, 3297 (2002).
[41]I. Brovchenko, A. Geiger, and A. Oleinikova, Phys. Chem. Chem. Phys. **6**, 1982 (2004).
[42]R. Biswas, J. E. Lewis, and M. Maroncelli, Chem. Phys. Lett. **310**, 485 (1999).
[43]J. E. Lewis, R. Biswas, A. G. Robinson, and M. Maroncelli, J. Phys. Chem. B **105**, 3306 (2001).
[44]T. Pradhan and R. Biswas, J. Phys. Chem. A **111**, 11514 (2007).
[45]T. Pradhan, P. Ghoshal, and R. Biswas, J. Phys. Chem. A **112**, 915 (2008).
[46]T. Pradhan, P. Ghoshal, and R. Biswas, J. Chem. Sci. **120**, 275 (2008).
[47]M. L. Horng, J. A. Gardecki, and M. Maroncelli, J. Phys. Chem. A **101**, 1030 (1997).
[48]K. Dahl, R. Biswas, N. Ito, and M. Maroncelli, J. Phys. Chem. B **109**, 1563 (2005).
[49]J. E. Lewis and M. Maroncelli, Chem. Phys. Lett. **282**, 197 (1998).
[50]R. Biswas, A. R. Das, T. Pradhan, D. Tauraud, W. Kunz, and S. Mahiuddin, J. Phys. Chem. B **112**, 6620 (2008).
[51]H. J. C. Berendsen, J. R. Grigera, and T. P. Straatsma, J. Phys. Chem. **91**, 6269 (1987).
[52]A. D. MacKerell, Jr., J. Wiórkiewicz-Kuczera, and M. Karplus, J. Am. Chem. Soc. **117**, 11946 (1995).
[53]M. P. Allen and D. J. Tildesley, *Computer Simulations of Liquids* (Oxford University Press, New York, 1987).
[54]C. W. Yong, *DL_FIELD–A Force Field and Model Development tool for DL_POLY* (STFC Daresbury Laboratory, Daresbury, 2010).
[55]G. Cinacchi, F. Ingrosso, and A. Tani, J. Phys. Chem. B **110**, 13633 (2006).
[56]N. Kometani, S. Arzhantsev, and M. Maroncelli, J. Phys. Chem. A **110**, 3405 (2006).
[57]W. Smith, T. R. Forester, and I. T. Todorov, *DL_POLY Classic* (STFC Daresbury Laboratory, Daresbury, 2012).
[58]S. Nose, J. Chem. Phys. **81**, 511 (1984).
[59]W. G. Hoover, Phys. Rev. A **31**, 1695 (1985).
[60]J. P. Ryckaert, G. Ciccotti, and H. J. C. Berendsen, J. Comput. Phys. **23**, 327 (1977).
[61]See supplementary material at http://dx.doi.org/10.1063/1.4943967 for steady-state abosorption and emission spectra of C153 in various concentrations of THF into water, behaviour of density, polarity, refractive index, and reaction field factor in the binary mixtures of THF/water and Diox/water, temperature effect on the absorption spectral frequency and width at the critical concentration of THF (0.225 mole fraction) into water, fitting parameters for excited-state lifetime decay and rotational anisotropy decay of C153 in both cycloether/water binary mixtures, representative rotational anisotropy decay of C153 in THF/water mixture, distribution of peak heights of radial distribution functions (RDFs) of water oxygen atoms in cycloether/water mixtures, RDFs between several atomic pairs of these solutions, and several dynamic heterogeneity parameters..
[62]T. M. Aminabhavi and B. Gopalakrishna, J. Chem. Eng. Data **40**, 856 (1995).
[63]F. E. Critchfield, J. A. Gibson, Jr., and J. L. Hall, J. Am. Chem. Soc. **75**, 6044 (1953).
[64]J. E. Lind and R. M. Fuoss, J. Phys. Chem. **65**, 999 (1961).
[65]M. L. Horng, J. A. Gardecki, A. Papazyan, and M. Maroncelli, J. Phys. Chem. B **99**, 17311 (1995).
[66]W. Hayduk, H. Laudie, and O. H. Smith, J. Chem. Eng. Data **18**, 373 (1973).
[67]H. Jin, G. A. Baker, S. Arzhantsev, J. Dong, and M. Maroncelli, J. Phys. Chem. B **111**, 7291 (2007).
[68]A. Das, R. Biswas, and J. Chakrabarti, J. Phys. Chem. A **115**, 973 (2011).
[69]A. Das, R. Biswas, and J. Chakrabarti, Chem. Phys. Lett. **558**, 36 (2013).
[70]J. P. Hansen and I. R. McDonald, *Theory of Simple Liquids* (Academic Press, New York, 1986).
[71]A. Luzar and D. Chandler, Nature **379**, 55 (1996).
[72]A. Luzar and D. Chandler, J. Chem. Phys. **98**, 8160 (1993).
[73]M. D. Ediger, Annu. Rev. Phys. Chem. **51**, 99 (2000).
[74]T. Pal and R. Biswas, J. Chem. Phys. **141**, 104501 (2014).
[75]A. Rahman, Phys. Rev. **136**, A405 (1964).
[76]S. Daschakraborty and R. Biswas, J. Chem. Sci. **124**, 763 (2012).
[77]S. Indra and R. Biswas, Mol. Simul. **41**, 471 (2015).
[78]E. Flenner and G. Szamel, Phys. Rev. E **72**, 011205 (2005).
[79]K. Kim and S. Saito, J. Chem. Phys. **133**, 044511 (2010).
[80]P. Schatzberg, J. Phys. Chem. **71**, 4569 (1967).
[81]C. Toninelli, M. Wyart, L. Berthier, G. Biroli, and J. Bouchaud, Phys. Rev. E **71**, 041505 (2005).
[82]C. Dasgupta, A. V. Indrani, S. Ramaswamy, and M. K. Phani, Europhys. Lett. **15**, 307 (1991).
[83]C. Donati, S. Franz, S. C. Glotzer, and G. Parisi, J. Non-Cryst. Solids **307-310**, 215 (2002).
[84]E. Flenner and G. Szamel, Phys. Rev. Lett. **105**, 217801 (2010).
[85]N. Lačević, F. W. Starr, T. B. Schrøder, V. N. Novikov, and S. C. Glotzer, Phys. Rev. E **66**, 030101 (2002).
[86]T. Pal and R. Biswas, J. Phys. Chem. B **119**, 15683 (2015).
[87]T. Abete, A. de Candia, E. Del Gado, A. Fierro, and A. Coniglio, Phys. Rev. Lett. **98**, 088301 (2007).
[88]S. E. Abraham and B. Bagchi, Phys. Rev. E **78**, 051501 (2008).
[89]T. Kawasaki and H. Tanaka, J. Phys.: Condens. Matter **23**, 194121 (2011).
[90]N. Lacevic, F. W. Starr, T. B. Schroder, and S. C. Glotzer, J. Chem. Phys. **119**, 7372 (2003).
[91]S. Franz and G. Parisi, J. Phys.: Condens. Matter **12**, 6335 (2000).
[92]L. Berthier, Phys. Rev. E **69**, 020201(R) (2004).
[93]R. Yamamoto and A. Onuki, Phys. Rev. E **98**, 3515 (1998).
[94]T. Pal and R. Biswas, J. Phys. Chem. B **119**, 15683 (2015).
[95]T. Pal and R. Biswas, Theor. Chem. Acc. **132**, 1348 (2013).
[96]D. K. Sasmal, A. K. Mandal, T. Mondal, and K. Bhattacharyya, J. Phys. Chem. B **115**, 7781 (2011).
[97]S. Ghosh, S. Chattoraj, R. Chowdhury, and K. Bhattacharyya, Rsc. Adv. **4**, 14378 (2014).
[98]S. Roy and B. Bagchi, J. Phys. Chem. B **118**, 5691 (2014).
[99]S. Roy and B. Bagchi, J. Phys. Chem. B **117**, 4488 (2013).
[100]S. Roy, B. Jana, and B. Bagchi, J. Chem. Phys. **136**, 115103 (2012).
[101]S. Chowdhuri and A. Chandra, J. Chem. Phys. **119**, 4360 (2003).
[102]M. S. Skaf, J. Phys. Chem. A **103**, 10719 (1999).
[103]G. M. Sando, K. Dahl, and J. C. Owrutsky, J. Phys. Chem. B **111**, 4901 (2007).